International Journal of Fatigue, Vol. 99, Part 1, June 2017, pp. 13-24
DOI:10.1016/j.ijfatigue.2017.02.010

Fatigue cracking behaviour of epoxy-based marine coatings on steel substrate under cyclic tension

T. Wu[1], P. E. Irving[1], D. Ayre[1], P. Jackson[2], F.Zhao[2]
[1] School of Aerospace, Transport, and Manufacturing, Cranfield University, Cranfield, Beds, MK43 0AL, United Kingdom
[2] AkzoNobel, Felling, Gateshead, UK

ABSTRACT

Strain controlled fatigue tests have been performed on two types of heavily filled epoxy corrosion protection coating sprayed onto a 6 mm steel substrate. Fatigue cycling was performed at R ratios of 0 and -1. The two coatings differed in their formulation and the major differences in mechanical performance were in their static strain to first crack development and their fracture toughness, where Coating A was significantly tougher than coating B. During strain cycling coating crack development was monitored using optical observations and surface replicas. It was found that in both coatings surface crack development began soon after the onset of cycling and proceeded via growth of surface channelling cracks and multiple initiation of new cracks. Detailed studies were made of crack development morphology and its relation to coating type and to the applied strain range. A definition of coating life as the first appearance of a 2 mm surface crack length was used. This represented the end of the life where the coating protected the substrate. Before this life was achieved, crack growth rates of single cracks were invariant with crack length. After this point further crack growth, multiple cracking and crack to crack interactions took place. Cracking in this region could be characterised with a new total crack length parameter shown to be strongly dependent on applied strain range.

KEYWORDS:

Epoxy coating; Fatigue life, Crack growth; Crack pattern; Fracture mechanics.

1. INTRODUCTION

Metallic engineering structures in marine applications are widely protected against corrosion by organic coatings [1]. A typical example of such coatings is the epoxy-based coatings used in marine structures, such as water ballast tanks (WBT) of double-hulled crude oil tankers [2]. Commercial WBT coatings are normally pre-qualified using IMO MSC215 (82) standard [3], based on the extent of coating failure and substrate corrosion of test samples under simulated thermal and humidity cycling. WBT coatings are subjected to cyclic strains in service generated primarily by repeated changes of temperature. Under these strains, pre-qualified coatings can still develop cracks at strain concentrations, such as the top of fillet welds [4]. This suggests that factors controlling coating cracking in service are poorly understood, and need further investigation as premature cracking can lead to rapid corrosion of the steel structures underneath, imposing a danger to tanker structural integrity [1]. Frequently, coating cracks reach lengths in meters before corrosion can be detected.

Fatigue behaviour of metallic and ceramic coatings for electronic and gas turbine applications has been widely studied [5–9]. Research into fatigue cracking of epoxy coatings on metal substrates including WBT coatings is on the other hand scarce. Lee *et al.* [4,10] investigated the fatigue failure of two WBT coatings of different thicknesses sprayed onto steel fillet welds under temperature cycles from 60 to - 20 °C. They found cracks were induced at the fillet welding line, and the life of the coatings was qualitatively correlated with coating thickness and coating ductility as measured in free film tests. Greater thickness and/or smaller free film ductility led to a shorter coating life. Using finite element analysis (FEA), Ringsberg and Ulfvarson [11] calculated the accumulated plastic strains of a WBT coatings on steel substrates in aged and unaged conditions under cyclic tensile strains. They used the fracture strain of aged and unaged free film coating samples as a failure criterion, and found that the aged coating had a shorter predicted life than the unaged one. They further claimed that coating embrittlement due to ageing was the main cause of premature cracking in service. However, none of

these papers on WBT coatings provides quantitative models to relate fatigue life to cyclic thermal strains, nor did they provide any information on fatigue crack development during strain cycling. This research aims to investigate quantitatively the fatigue life of WBT coatings under mechanical strain cycles, and will characterise fatigue crack growth in coatings.

Fracture mechanics models for cracks in coatings have been developed by a number of workers [12,13]. In theory [13], fracture of coatings originating from a surface defect under normal stresses can be simplified as a 2D process of crack penetrating towards the interface in plane strain, followed by a 3D process of crack channelling parallel to the coating plane. Figure 1 (a & b) illustrates these two processes. This approach has been applied to explain and predict the static strain to failure of coatings on substrate by Chai [14] and Wu *et al.* [15], who found the predicted values were close to the measured values. Wu *et al.* [15] also found that coating failure under static strains was likely to be initiated by regions of de-cohered large particles (60 – 70 μm), which merged with the coating surface.

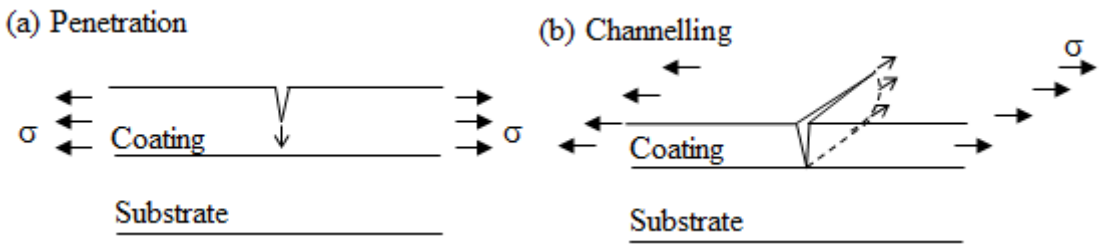

Figure 1. Illustrations of (a) crack penetration, (b) crack channelling under a uniform remote tensile stress. [15]

In contrast to uniaxial mechanical strains, coating thermal strains in service are bi-axial. For the same strain, the corresponding coating stress produced by uniaxial mechanical loading will be smaller than that produced by biaxial thermal strains as indicated by equations (1) and (2) [16].

$$\sigma_{\text{uniaxial}} = E\varepsilon \tag{1}$$

$$\sigma_{\text{biaxial}} = \frac{E\varepsilon}{1-\nu} \tag{2}$$

Here, E and ε are Young's modulus and strain, and ν is Poisson's ratio. A further difference between thermal and mechanical strains is that testing under mechanical tensile loads will subject substrates and coatings to identical strains; hence substrates experience large stresses which may cause their failure. In the absence of mechanical loads, under thermal cycling of coated samples force balance determines that substrate strains are small and coating strains large and there is little possibility of substrate failure. However, reproduction of service thermal cycles in the laboratory is experimentally complex and difficult to model. To test the response of the coating to cyclic strains, application of mechanical strains at constant temperature is the simplest method. In the current work, uniaxial mechanical strain cycles were applied to two epoxy-based coating formulations supported by steel substrates. The development of cracks on the coating surface was observed to identify coating failure processes under cyclic strains.

2. EXPERIMENTAL

2.1. Materials

Two heavily filled epoxy coatings, named coating A and coating B were studied. Before curing, the coatings were viscous liquids with high solvent contents. The substrate was 5.5 mm thick steel plate to BSEN 10225 grade S355K2+N. Tensile tests reported fully in [15,17] showed that the yield and ultimate strength of the substrate steel were 420 MPa and 560 MPa [17]. The coating properties of Young's modulus (E), static strain to the onset of first crack (ε_f) and fracture toughness (G_C), at 23°C as well as the glass transition temperature (T_g), are shown in Table 1 [17]. Both coatings have the same modulus, while coating A has 3 times the facture toughness of coating B and a significantly greater strain to first crack. The stress-strain curves of both coatings in a free standing film form exhibited some degree of non-linearity before fracture, the details can be found in [15,17].

	E (GPa)	T_g (°C)	ε_f (%)	G_C (J/m^2)
Coating A	5.2	65	1.04	228
Coating B	5.2	69	0.64	76

Table 1. Young's modulus, glass transition temperature, and static strain to first crack of the coatings [17] .

2.2. Sample Manufacture

Fatigue test sample substrates were 5.5 mm thick and of the geometry shown in Figure 2 with a gauge length of 12.5 mm and width of 12.5 mm. The sample surfaces were shot-blasted to Sa2.5 [18]. One surface was sprayed with coating, nominally 300 µm in thickness. The coatings were cured at ambient temperature (~ 23 °C) for 7 days, followed by 2 days post-curing at 100 °C. The post-cure process was to ensure full curing, simulating a fully cured coating in service. The coating thickness of each sample was measured using a coating thickness gauge. The average thickness was 300 ± 25 µm for coating A and 350 ± 27 µm for coating B. Due to the mismatch between the coefficients of thermal expansion of coating and substrate, thermal residual stresses were developed in both coatings at room temperature. The residual stress values for both coatings at 23 °C, cooled from 100 °C, were measured using a bilayer beam deflection technique [17], widely used for coating internal stress measurement [19,20]. For coatings A and B, the thermal residual stresses were respectively 10.9 MPa and 14.3 MPa [17]. Before testing, samples were conditioned thermally at 100 °C for 30 minutes. This was done to restore the original coating properties, as modulus, toughness and residual stress values could change during storage at room temperature due to physical ageing [21]. All samples had the test start within 8 hours after conditioning.

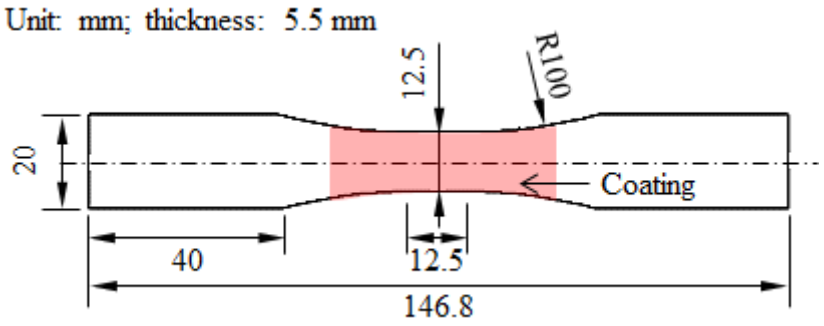

Figure 2. Dimensions of fatigue test samples

2.3. Test Procedure

Strain-controlled fatigue tests were performed at ambient temperature (~ 23 °C) on a servo- hydraulic digitally controlled test machine. The controlling extensometer had a gauge length of 12.5 mm and was attached to the uncoated side of the samples. Cycling was performed under R ratios (R = $\varepsilon_{min}/\varepsilon_{max}$) of -1 (fully reversed tension – compression) and 0 (zero to tension). Table 2 shows the test matrix performed. The strain amplitudes were selected based on the following requirements: 1) the maximum strains of the strain amplitudes must be smaller than the coating static strain to first crack shown in Table 1; 2) the strain amplitudes must be able to cause coating fatigue cracking before the commencement of substrate fatigue cracking; 3) a theoretical calculation [17] shows that the current coatings can develop a thermal strain from 0.25% to 0.52% in service at 0 °C, the strain amplitudes should also be representative of this range.

Coating type	R ratio	Sample label	Strain amplitude $\Delta\varepsilon/2$ (%)	Number of samples
Coating A	-1	FFA 1 ~ FFA 7	±0.45 ~ ±0.60	7
	0	FTA 1 ~ FTA 8	±0.40 ~ ±0.55	8
Coating B	-1	FFB 1 ~ FFB 12	±0.16 ~ ±0.45	12
	0	FTB 1 ~ FTB 9	±0.20 ~ ±0.30	9

Table 2. Matrix of fatigue tests of both coatings

Since the substrate had much greater modulus and thickness than the coatings, the ratio of the product of cross-section area and modulus of the substrate to that of the coating was about 760, thus only 0.13%

of the load was due to the coating. Changes in the load response of the samples to the imposed strain will be overwhelmingly caused by changes in the substrate cyclic stress-strain properties. Any changes in coating stress-strain properties will not be detectable. Similarly changes in sample compliance caused by coating crack development will not influence the strains imposed by the substrate on the coating.

Coating crack development during fatigue was recorded primarily using a Microset RT101 surface replication compound. Tests were paused at the mean strain to allow replica application, and then resumed after 5 minutes when the replica was fully cured and removed. Intervals of 10 cycles or 100 cycles, were used in the beginning of the tests. When cracks $\geq$ 1 mm were seen, cycle intervals between replicas were increased. The coating failure criterion was chosen to be the appearance of the first 2 mm long surface crack. This was decided by assuming coating cracks initially have a semi-circular crack front; a through-thickness crack will have therefore a minimum surface length of 0.6 mm in a 0.3 mm thick coating. Once a through-thickness crack is formed at surface length of 0.6 mm, the corrodant can penetrate to the substrate and the coating has in theory failed. Selection of a slightly larger 2 mm surface crack as the definition of failure is a more robust practical criterion. The cycle number at the failure point is defined as the fatigue life. The sensitivity of fatigue life to the failure criterion assumed will be discussed later. To study the development of coating cracks, cycling was continued after the failure point, and crack growth monitored until either failure of steel substrate or the "saturation" of coating fatigue cracks, where the entire sample surface was covered by cracks that did not appear to grow in either length or number with further cycling.

After the tests, the surface replicas were examined using an optical microscope. Coordinates of the two ends of each crack were recorded, and the line distance between the ends was used as the crack length. The measuring error of this method was determined to be ± 2 μm using a standard line sample with a known length of 100 μm. For the coating sample tested at an amplitude of 0.24% (R = -1), a digital camera (1M pixels) was used to characterise surface crack development. An alcohol based blue ink

was used to enhance the contrast between cracks and coating. Due to optical imaging difficulties, cracks in coating A were recorded using replicas only.

3. RESULTS

3.1. General Attributes

Fatigue cracking of coatings commenced with the appearance of one or two cracks within the sample gauge length after an initial short incubation period. At bigger strain amplitudes, fewer cycles were needed for this to occur. For example, cracks were visible after 200 cycles in coating B under a fully reversed strain amplitude of ±0.45%, while they were first seen after 3000 cycles under a strain amplitude of ±0.24%. The crack length at this stage ranged from 100 to 300 μm. For both coatings A and B, as cycling continued, existing cracks grew longer, whilst new cracks appeared at other sites. This trend continued with further cycling; eventually the coatings developed cracks with a pattern with multiple parallel cracks perpendicular to the loading direction. An example of coating crack development in coating B is shown in Figure 3, tested under fully reversed cycling at a strain amplitude of ±0.24%. The red arrows point to the initial observation of cracks. Black dots, visible on the coating surface in Figure 3, were later found to be surface pores of 100 μm in diameter. They were not visible on the coating surface before cycling commenced, see Figure 3a, and were not observed to initiate cracks.

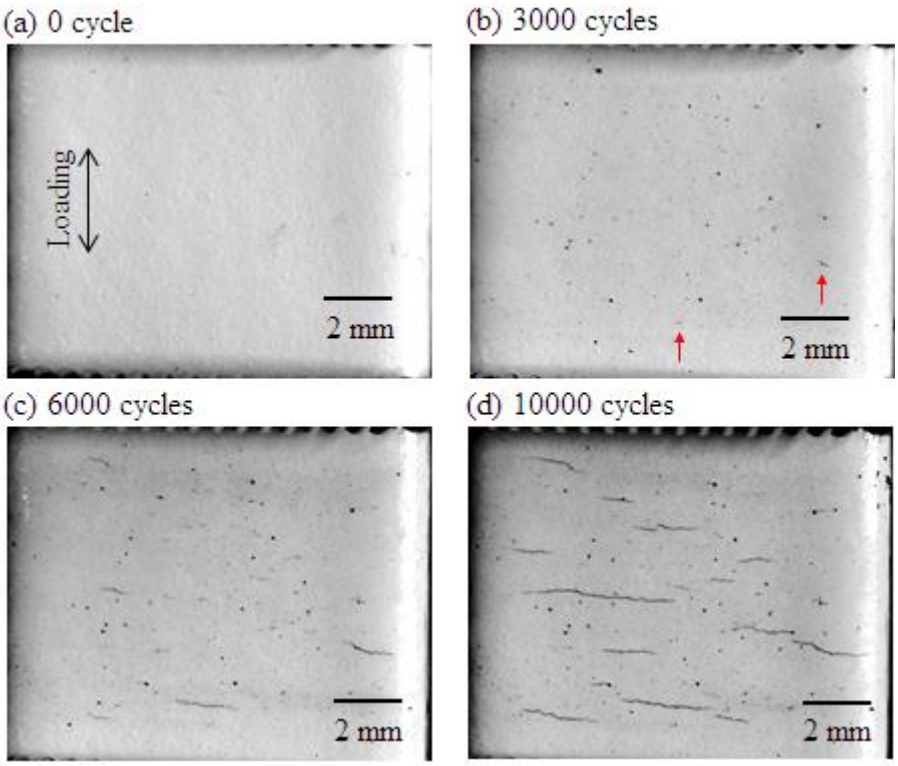

Figure 3. Surface fatigue crack development of a coating B sample tested under a strain amplitude of ± 0.24% (R = -1).

Fatigue crack development in coating A samples was observed in replicas under optical microscopy. As an example, Figure 4 shows the growth of a crack in coating A, from a length of 0.4 mm at 100 cycles to 1.5 mm at 300 cycles, under a strain amplitude of ± 0.5% (R = 0). The crack development shown in Figure 4 is very irregular with many local deviations from the primary crack plane, and occasional examples of crack bifurcation around obstacles in the crack path; the cracks later recombining.

The cyclic strain values applied (between ±0.16% and ±0.6%) are considerably more than the fatigue limit of the substrate steel. Consequently, after sufficient test cycles, fatigue failure of the steel substrate took place. This occurred at lives ranging from 150 to 1.5×10^5 cycles depending on the applied strain. Substrate failure imposed an upper limit to the coating lives which could be investigated. As macroscopic substrate cracks would change the strain distribution in the coating, when a substrate fatigue crack was observed the test was terminated and coating crack development could not be

investigated further. The relationship between strain amplitude and life for the substrate is plotted in Figure 5a for both R ratios. This shows the life of substrate is insensitive to R ratio between -1 and 0 at these short and intermediate fatigue lives.

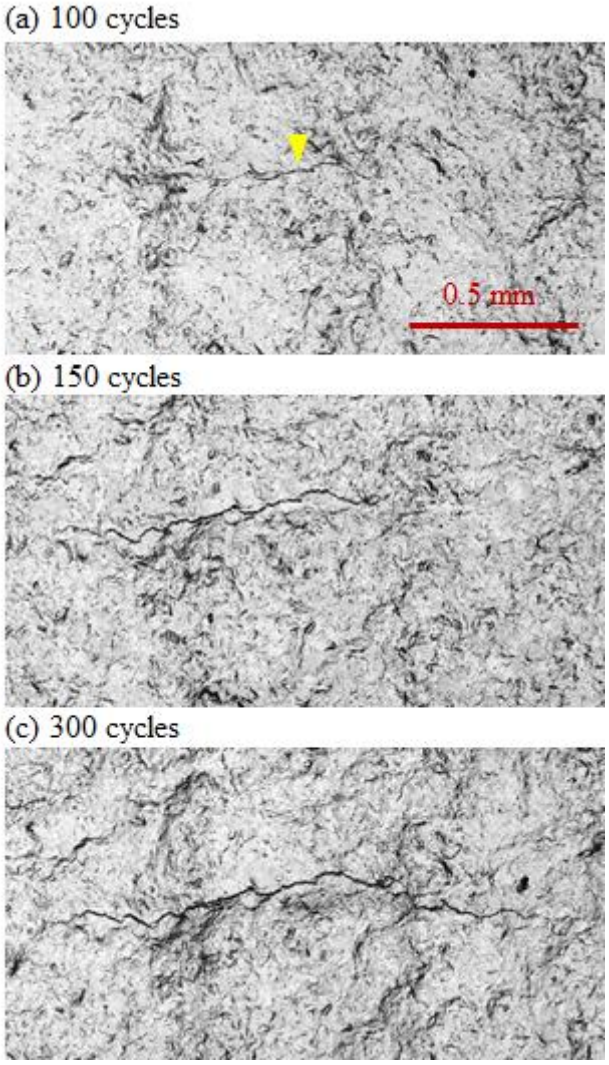

Figure 4. Replica images of the development of a single fatigue crack on a coating A sample under a strain amplitude of ±0.5% (R = 0).

The strain – life behaviour of both coatings to the first 2 mm crack is plotted in Figure 5b. The substrate strain - life line, also shown on the figure, defines an upper limit of cycle number beyond which coating life could not be studied. Figure 5b shows that significantly larger strain amplitudes are required to produce the same life in coating A than in coating B. The only data point that allows direct comparison between the lives of both coatings is at a strain amplitude of 0.45%, where the life of coating A is

about 250 times that of coating B. The data points can be fitted to an equation similar to the Coffin-Manson expression for the relation between plastic strain and life for metals [22]. Equation (3) uses total strain amplitude ($\Delta\varepsilon/2$) instead of plastic strain, and ε_t' and n are constants determined by statistical best fitting, and N is the life to the first 2 mm coating crack. The best fit lines for equation (3) are shown by the dashed lines in Figure 5. The values for ε_t' and n are shown in Table 3.

$$\frac{\Delta\varepsilon}{2} = \varepsilon_t'(N)^n \tag{3}$$

	R ratio	ε_t'	n
Coating A	-1	6.3×10^{-3}	$- 3.9 \times 10^{-2}$
	0	8.2×10^{-3}	$- 9.1 \times 10^{-2}$
Coating B	-1	5.5×10^{-3}	$- 9.9 \times 10^{-2}$
	0	2.8×10^{-3}	$- 3.0 \times 10^{-2}$

Table 3. Resultant constants determined by fitting the coating fatigue life data to equation (3).

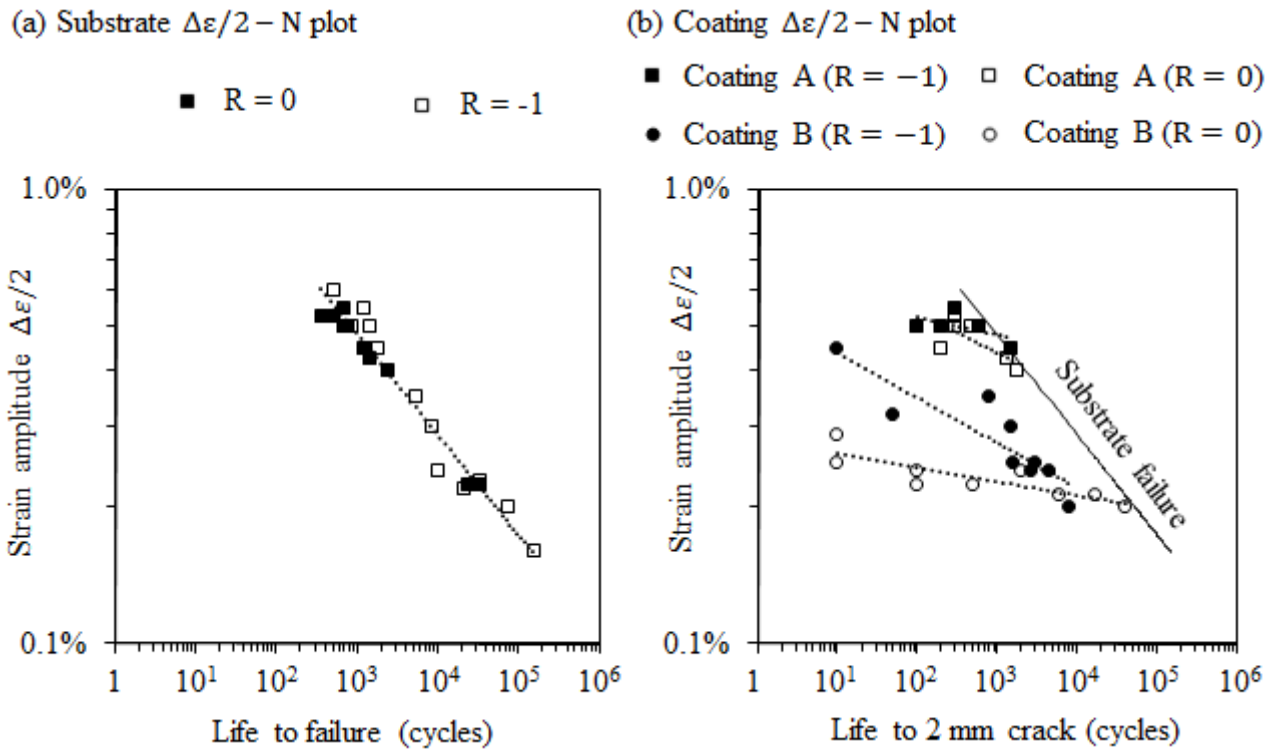

Figure 5. Strain amplitude vs. fatigue cycles for (a) steel substrate, and (b) coatings. The dashed lines are best fits to equation (3).

Figure 6 plots life against maximum strain rather than amplitude and shows that coating B has significant sensitivity to R ratios between 0 and -1 over the lives studied. The dashed lines are best fit

lines for a power-law relationship. Life is sensitive to maximum strain (ε_{max}) rather than strain range. Coating A shows insensitivity to R ratio as can be seen in Figure 5b. Crack development to the first 2 mm crack was limited to a few cracks visible on each sample. The crack development process up to 2 mm and beyond was studied to provide data on crack growth rates.

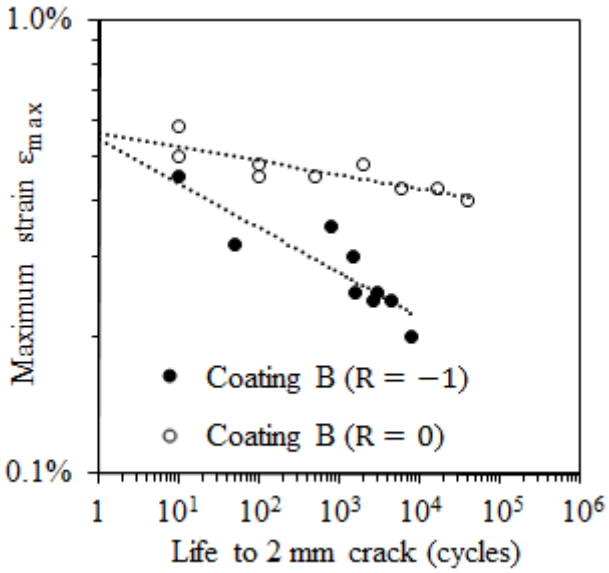

Figure 6. Maximum strain vs. cycles to first 2 mm crack of coating B tested at R values of 0 and -1.

3.2. Crack Growth observations

Crack length development as a function of cycle number in 5 single cracks all from a specimen of each coating is shown in Figure 7. The dashed lines are best linear fits. These two samples were not tested at the same strain amplitude, and should not be compared directly. For each of the single cracks in both the samples shown in Figure 7, the crack length increases linearly with increasing cycle number. This indicates that the growth rate of single cracks is independent of crack length. However, crack growth rates varied significantly from crack to crack within individual samples. The growth rate of the fastest growing crack could be 6 times greater than that of the slowest.

To characterise the variability of single crack growth rates on the same samples, a mean crack growth rate and standard deviation were calculated using the data in Figure 7. Mean growth rates for the selected strain amplitudes were 3 ± 1.3 μm/cycle for coating A and 0.8 ± 0.6 μm/cycle for coating B.

The uncertainties are standard deviations, which can be as high as 75% of the mean value in the case of coating B.

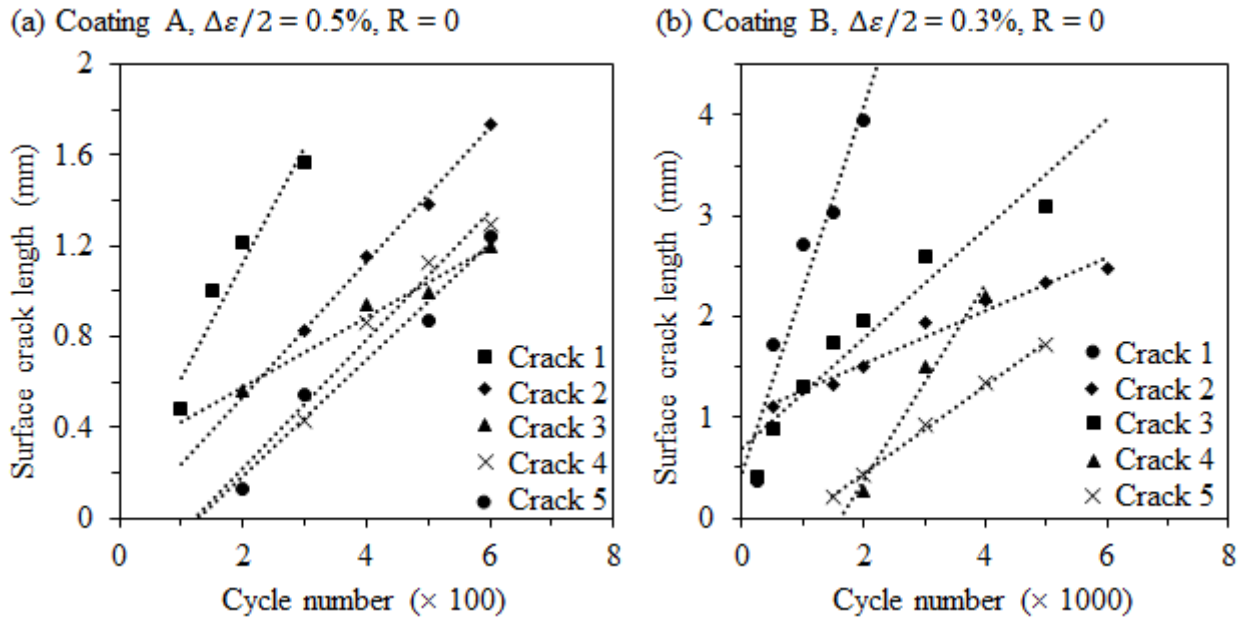

Figure 7. Crack length vs. cycle number of single cracks before interaction. (a) Coating A sample tested at an amplitude of ±0.5% (R = 0); (b) Coating B sample tested at an amplitude of ±0.3% (R = 0). The dashed lines are best linear fits to the data.

Figure 7 shows that different cracks achieved a defined length at very different cycle numbers depending on when the crack had initiated and the growth rate that it adopted. Figure 7b shows that crack 1 achieved 2 mm length at about 1000 cycles, while the other cracks achieved this length at much greater cycles (up to 6000 cycles for crack 5). Figure 7a shows a similar trend in coating A, but in this sample the failure crack length of 2 mm has not yet been achieved in any of the cracks.

When multiple cracks were present, the tips eventually interacted with other cracks when they grew into their vicinity and individual crack growth rates were significantly influenced. For example, Figure 8a illustrates a long centre crack with two nearby cracks on either side. The centre crack was first observed at 100 cycles, and both ends of the crack at 300 cycles are shown in Figure 8 b and c. The tips of the centre crack are indicated by red arrows, and two separate cracks within 0.4 mm distance are indicated by blue arrows. The length of the centre crack as a function of cycle number is shown in

Figure 9. The dashed lines going through the data points are the best linear fits of the first and last 4 data points, they intersect at about 280 cycles. A red vertical dashed line is shown in Figure 9 to mark the cycle number where crack interaction was observed at 300 cycles. The crack growth rate was significantly slowed after interaction as the crack tips began to influence each other.

Beyond the point of crack interaction, growth of individual cracks was not representative of general crack development. To quantify global fatigue crack development, a total crack length (L_{total}) parameter was defined as the sum of the lengths of all cracks in an 8 mm × 12.5 mm region within the gauge length,

$$L_{total} = \sum_{i}^{n_i} l_i \tag{4}$$

where, l_i is the length of an individual crack, and n_i is the number of cracks. In all samples L_{total} increased with test cycle number, and the rate of L_{total} development increased with increasing strain amplitude. Examples of L_{total} development can be found in Figure 10. The L_{total} of most coating A samples increased almost linearly with cycle number till the end of the test. In contrast, the L_{total} of coating B samples initially increased linearly with cycle number, and then slowed down. The cause of the slowdown was probably interaction with other nearby cracks at large values of L_{total}. This was not observed in coating A, as the tests were terminated before saturation had been reached because of substrate failure.

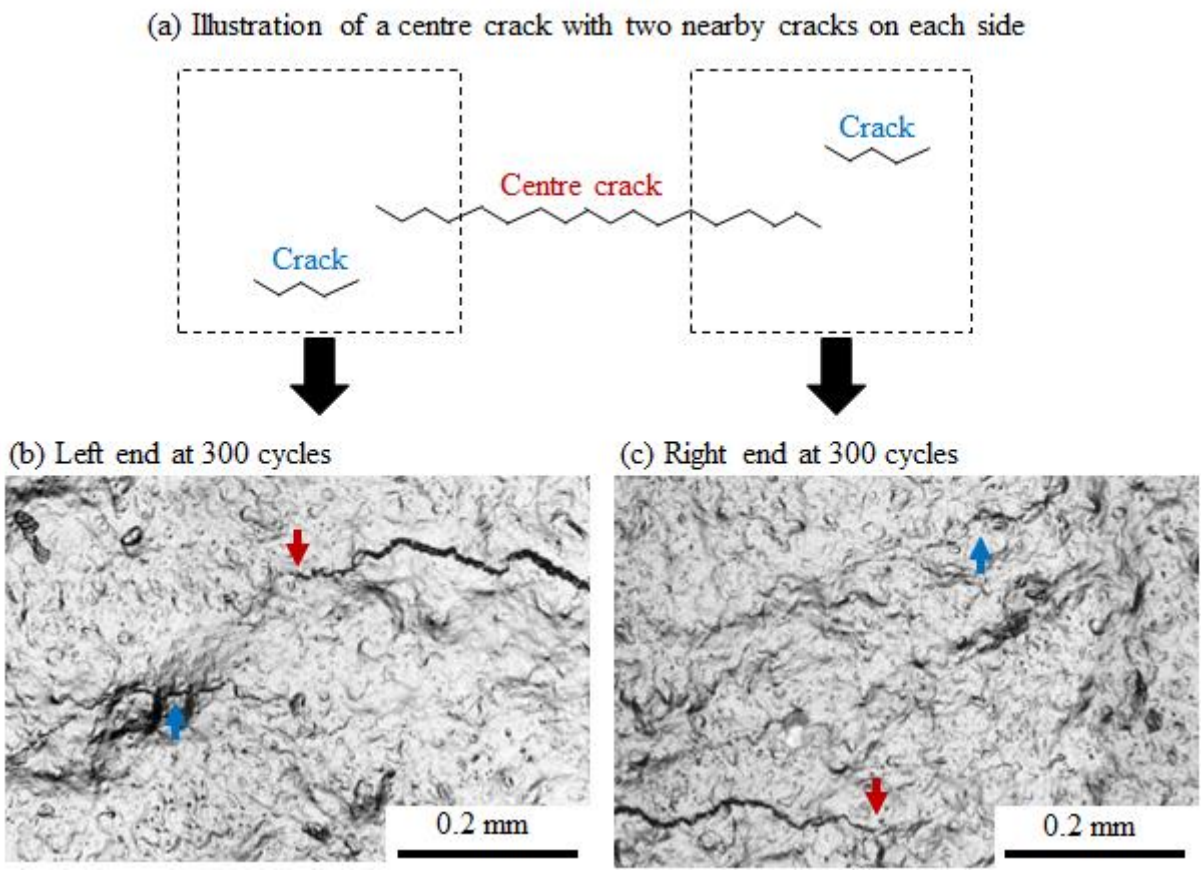

Figure 8. (a) Schematic diagram of crack locations. (b & c) Surface replicas of coating A sample ($\Delta\varepsilon$ = 0.5%, R = 0, after 300 cycles) showing the centre crack indicated by red arrows, with ajacent cracks at each end (blue arrows). Development of the central crack with cycling shown in Figure 9 below.

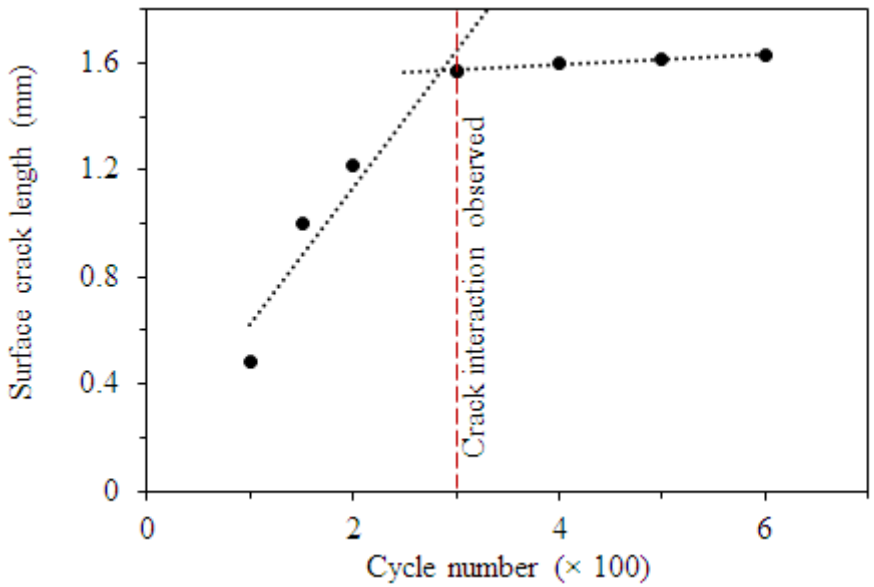

Figure 9. Development of the length of the centre crack shown in Figure 8 b and c as a function of cycle number. The red vertical dashed line marks the cycle number where crack interaction was first observed.

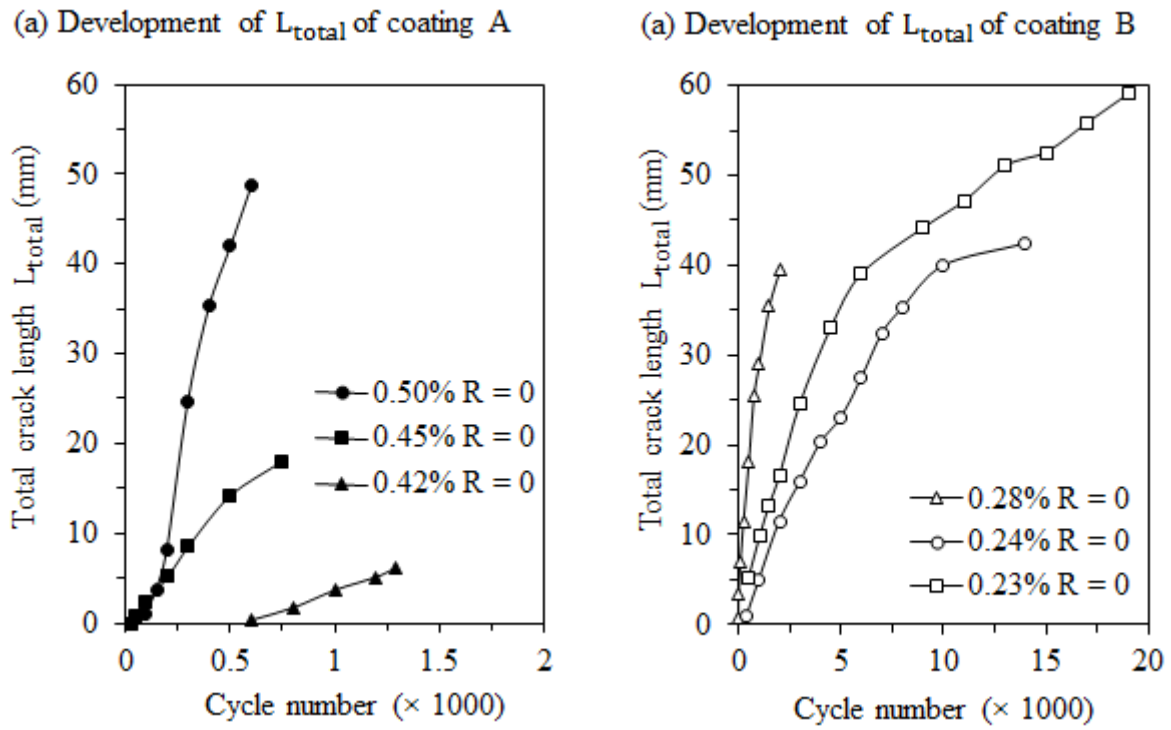

Figure 10. L_{total} plotted against cycle number, (a) for coating A and (b) for coating B tested at three strain amplitudes.

3.3. Crack morphology and interaction

To quantify crack morphology, crack number and average crack length of 6 coating A samples and 4 coating B samples, tested at different strain amplitudes were measured and are plotted in Figure 11 as a function of L_{total}. This shows very different crack development in the two coatings. At the same L_{total} the number of cracks in coating A is about 3 to 4 times that in coating B; whilst the average crack length in coating A is about a quarter to one third of that in coating B.

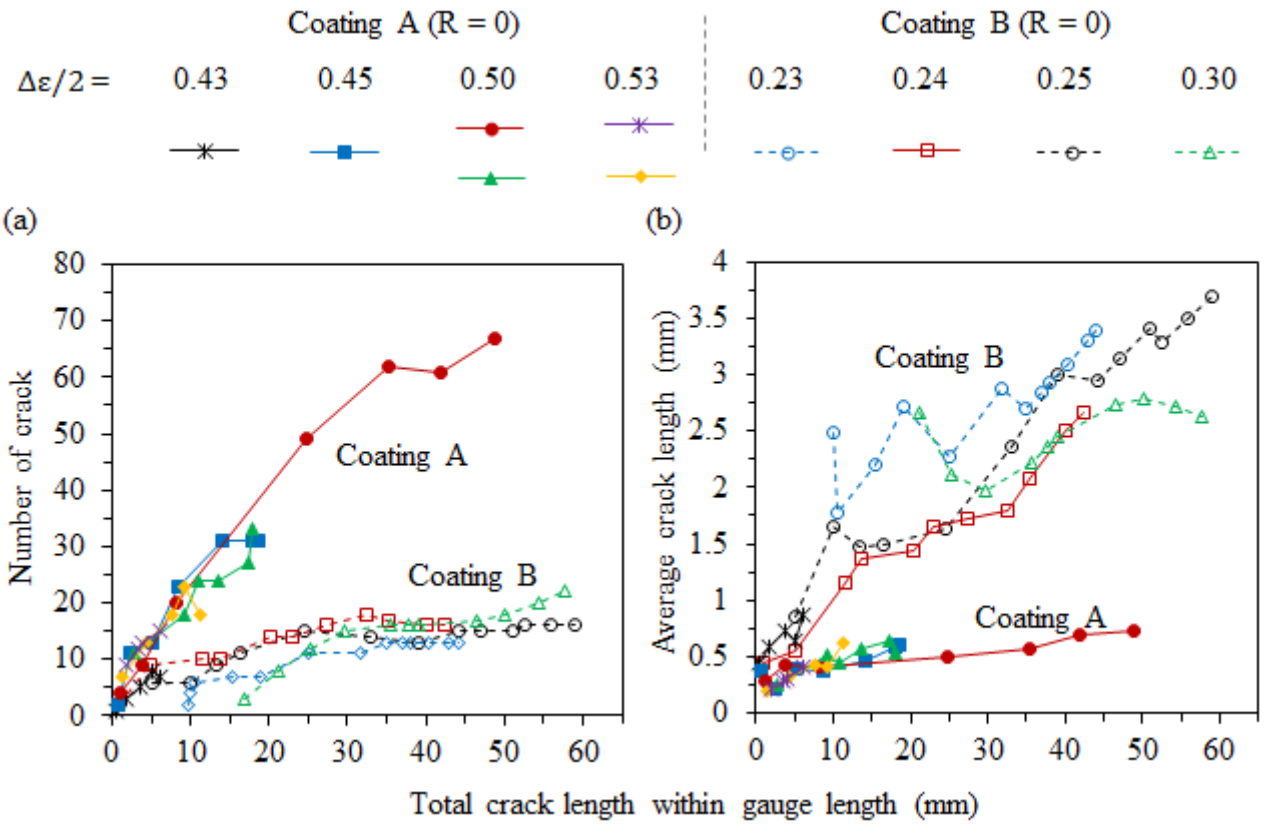

Figure 11. (a) Development of number of cracks and (b) Development of average crack lengths as a function of L_{total} in coatings A and B.

The extent of crack interaction was characterised following guidelines proposed by Xia and Hutchinson [23], in which a crack tip can be treated as non-interacting if 3 criteria are met, see Figure 12. In Figure 12, a is the crack length, H is the distance between two parallel adjacent cracks, d is the horizontal distance between the confronting crack tips of two parallel adjacent cracks, l_r is a reference length described by equation (5).

$$l_r = \frac{\pi}{2} g(\alpha, \beta) h \tag{5}$$

Here, $g(\alpha, \beta)$ is a term determined by the stiffness mismatch between coating and substrate for a through-thickness channelling crack, and the details of it can be found in Beuth [12], and h is the coating thickness. The l_r of coatings A and B was calculated as 0.32 mm and 0.38 mm respectively.

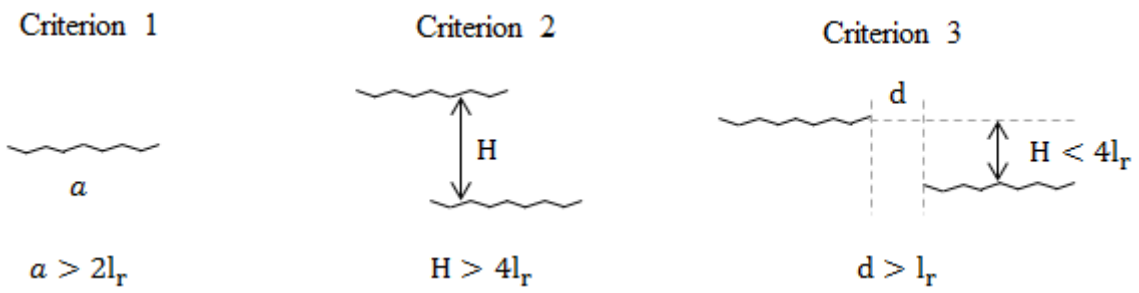

Figure 12. Illustrations for the criteria of a non-interacting crack tip suggested by the results of [23].

For crack tips to be non-interacting, criterion 1 requires a single crack to be longer than twice l_r, criterion 2 requires a distance between two parallel and adjacent cracks to be as least 4 times l_r, and for criterion 3 the horizontal distance d between crack tips must be greater than l_r. Using these criteria, the number of non-interacting crack tips (NNIT) and the total number of crack tips (twice the crack number), were quantified. The values are shown as a function of L_{total} in Figure 13.

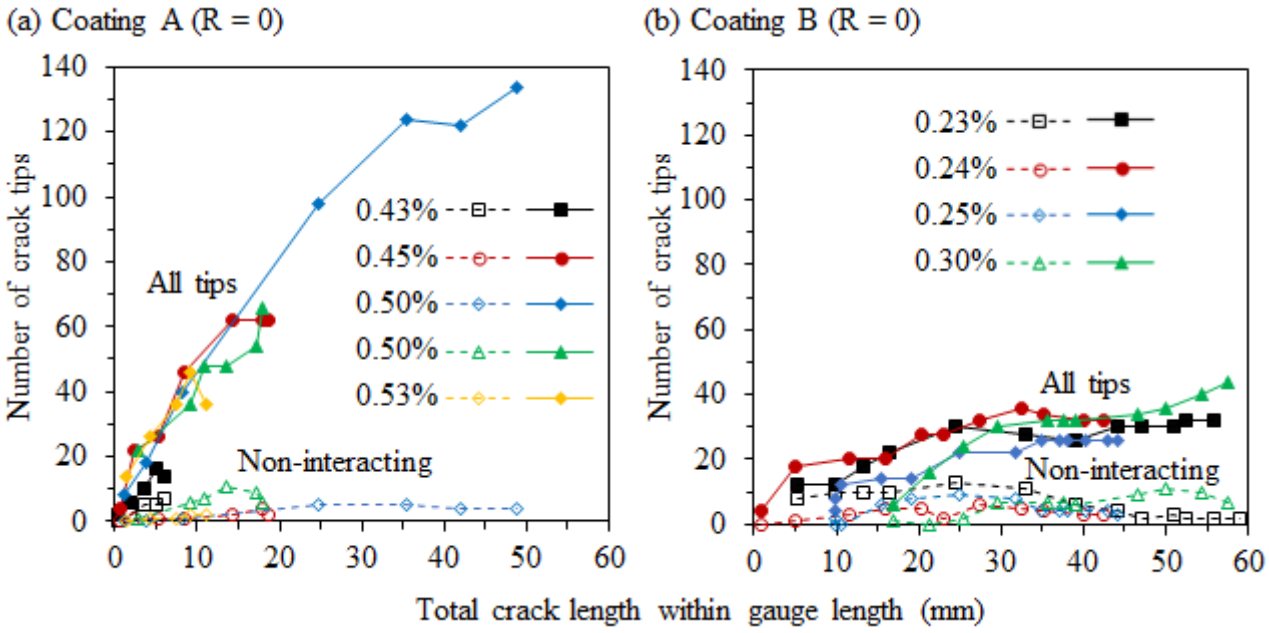

Figure 13. The development of the total number of crack tips (solid points) and the number of non-interacting cracks (open points) plotted against L_{total} for coatings A and B.

The NNIT of both coatings increases in the beginning of crack development, and as the total crack length increases further the NNIT decreases. In contrast, the total number of crack tips increases monotonically. Over the entire total crack length range, the NNIT of coating A largely stays below 5,

while the NNIT of coating B is below 10. A more significant difference between the coatings is the difference between the total number of crack tips and NNIT. For coating A, there is a large difference between these two, increasing with increased total crack length. Coating B has the same trend, but the difference between the total number of crack tips and NNIT is significantly smaller than in coating A. Crack interaction is much more pronounced in coating A than in coating B.

3.4. Crack Growth Rates

A total crack growth rate (dL_{total}/dN) was defined as the slope of the initial linear portions of the total crack length – cycles data such as those shown in figure 10. An averaged non-interacting crack growth rate (dL_{avg}/dN) was defined as the mean value of the growth rates of 5 non-interacting cracks such as those seen in Figure 7. The values of dL_{total}/dN and dL_{avg}/dN of samples which had comprehensive growth data available are plotted against strain range ($\Delta\varepsilon$), in Figure 14. Each point represents data from one individual test sample tested at a single strain range. It was found the data could be best fitted to a power-law relationship of the form:

$$\frac{dL_{total}}{dN} \text{ or } \frac{dL_{avg}}{dN} = C'(\Delta\varepsilon)^{m'} \quad (6)$$

where, C' and m' are constants determined by data fitting, m' being the line gradient. Values for C' and m' from the fitting are shown in Table 4.

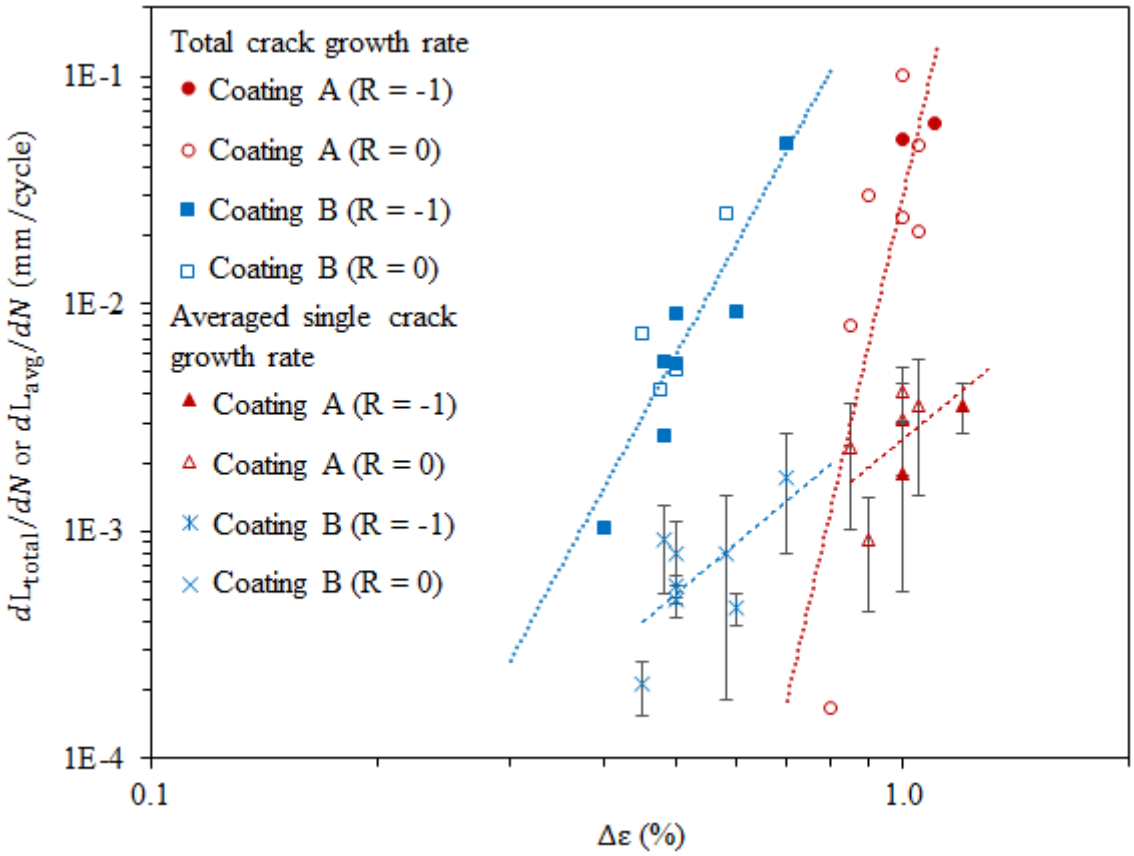

Figure 14. Total crack growth rate (dL_{total}/dN) and averaged non-interacting crack growth rates (dL_{avg}/dN) as a function of strain range ($\Delta\varepsilon$).

Coating type	dL_{total}/dN		dL_{avg}/dN	
	C′ (mm/cycle)	m′	C′ (mm/cycle)	m′
A	0.031	14.4	0.003	2.71
B	0.414	6.09	0.004	2.78

Table 4. Empirical constants of the fitted lines in Figure 14 calculated using equation (6).

In Figure 14, data points from tests at R ratios of -1 and 0 both fall on the same line and there is no obvious effect of mean stress on crack growth rates. Within the strain ranges studied, coating A was more resistant to fatigue crack growth than coating B, as coating B had dL_{total}/dN values up to 500 times that of coating A for the same strain range. The large values of m′ for (dL_{total}/dN) show that total crack growth rates in both coatings are highly sensitive to strain range. Values of dL_{avg}/dN are much smaller than dL_{total}/dN and have reduced sensitivity to strain range via the smaller values of the exponent m′.

4. DISCUSSION

Surface observations made during fatigue testing demonstrate that coating crack development begins early in the test. If an initiation life prior to the onset of cracking exists, it is a small fraction of total life. As cycling continues existing cracks grow longer, and new cracks are initiated at fresh locations, eventually covering the entire sample surface. Initial growth of a new crack proceeds at a constant rate, but eventually adjacent crack tips become sufficiently close for interaction to occur and the crack growth rate reduces. However crack numbers continue to grow. The two coatings differ in their responses to strain cycles with the tougher coating A withstanding 2-3 times the strain range to achieve the same fatigue life than the less tough coating B.

As coating crack growth begins soon after the start of cycling, there is no obvious criterion for sample failure other than the life at which the first coating crack is detected. This might be a few 10s of cycles for large strain ranges, or some hundreds of cycles for smaller strains and longer lives. The measured life will depend on the surface crack length used as the failure criterion. Using a shorter or a longer crack length would result in a shorter or longer life. Using the growth data of crack 1 in Figure 7b as an example, the cycles to achieve a first crack length of 2 mm in coating B is 500 cycles, for a crack length of 4 mm the life will be 2,000 cycles and even longer for a 10 mm crack. Similar considerations apply to coating A crack growth. Crack interaction effects will intervene at longer crack lengths and will complicate the definition of life. Use of the total crack growth rate parameter (dL_{total}/dN), representing a population of cracks will be more relevant at longer crack lengths. From the point of view of coating service performance, the important issue will be the corrosion resistance of the coating, and total crack growth increase will be related to decline in corrosion resistance. As coating fatigue life measured by any of these criteria is dependent on crack growth rates, the relation between applied strain range and growth rates (Figure 14 and equation 6) is hence of considerable importance.

Equation (6) is similar to the well-known relationship [24], between fatigue crack growth rate and stress intensity range ΔK for metals, or ΔG the strain energy release rate range, for fatigue crack growth in metallic [22] and brittle polymers [25], and for fatigue delamination crack growth in polymer composites [26],

$$\frac{\mathrm{d}a}{\mathrm{dN}} = \mathrm{C}(\Delta \mathrm{G})^{\mathrm{m}} \tag{7}$$

where a is delamination length and length, C and m are empirical constants.

For the case of channelling cracks in coatings, Beuth [12] has demonstrated that the strain energy release rate G is given by:

$$\mathrm{G_{ch}} = \frac{1}{2}\frac{\pi\sigma^2 \mathrm{h}}{\mathrm{E_c}}\mathrm{g}(\alpha, \beta, a/\mathrm{h}) \tag{8}$$

Where σ is the coating stress, h coating thickness, $\mathrm{E_c}$ coating Young's modulus and g(α,β,a/h) is a function of the Dunders parameters [27] α and β, reflecting the elastic misfit between the coating and the substrate, and a the crack depth, and h the coating thickness. Surface crack length l does not appear in this equation and crack driving force G is therefore independent of surface crack length. For a channelling crack of specified substrate and coating materials, and of full depth in a coating of fixed thickness (hence $\mathrm{a} = \mathrm{h}$), the function g will be constant, as will h and $\mathrm{E_c}$. Hence for these conditions:

$$\mathrm{G_{ch}} = \frac{\sigma^2}{\mathrm{E_c}} \times \mathrm{C_1} \tag{9}$$

where $\mathrm{C_1}$ is a constant. For elastic conditions in the coating, $\sigma = \varepsilon \mathrm{E_c}$, and

$$\mathrm{G_{ch}} = \varepsilon^2 \mathrm{E_c} \times \mathrm{C_1} \tag{10}$$

Under cyclic deformation replacing values of strain energy release rate G and strain ε with the corresponding ranges,

$$\Delta G_{ch} = \Delta\varepsilon^2 E_c \times C_1 \quad (11)$$

Hence the applied strain range Δε in figure 14 is closely related to ΔG_{ch} the strain energy release rate for channelling cracks, and the observed relation equation (6) between Δε and channelling crack growth rates can be understood in terms of equation (11) the relation between ΔG and Δε. A constant Δε leads to a constant ΔG_{ch}, which would further lead to a constant crack growth rate, such as those observed in Figure 7.

However, at the applied strain ranges used in these tests, coating stress-strain behaviour is non-linear [15,17]. In addition, the steel substrate undergoing cyclic plasticity, will change the values of the Dunders parameters from their elastic values. In these circumstances, it is appropriate to use the non-linear J integral [22] rather than the elastic G to characterise channelling crack growth rates. For fatigue crack growth in materials undergoing non-linear deformation, ΔG can be replaced with ΔJ, the J-integral range [28–30], and thus equation (7) can be rewritten as equation (12).

$$\frac{da}{dN} = C(\Delta J)^m \quad (12)$$

The total crack growth rate and the average single crack growth rate can be plotted using equation (12) with da/dN replaced by dL_{total}/dN and dL_{avg}/dN provided that values of ΔJ_{ch} can be calculated.

Approaches for calculation of ΔJ for cracks in monolithic samples undergoing elastic-plastic (non-linear elastic) cyclic deformation have been established previously by a number of researchers [28–31]. ΔJ can be calculated via a determination of J at the maximum hysteresis loop tip, with the loop being offset to allow the minimum hysteresis loop top to coincide with the origin [17]. J values of coating cracks will be influenced by the cyclic stress-strain behaviour of the substrate via changes to the Dundurs parameters. Substrate cyclic stress-strain curves were obtained experimentally during the fatigue tests. Coating stress-strain behaviour was assumed to be cyclically stable and stress-strain curves obtained from monotonic tests of coating free films reported in [17] were used. All stress-strain

curves were represented via Ramberg-Osgood equations. J values of the coating channelling cracks at Δε values up to 1.5% were calculated using the numerical procedure within ABAQUS FE analysis package [32]. The detailed procedure is described in [17].

Figure 15 shows values of dL_{total}/dN and dL_{avg}/dN replotted against ΔJ_{ch} again on a Log-Log scale. Once again a linear relation is obtained. A statistical best fit gives the constants C and m in table 5. The trends of the data are broadly similar to those shown in the strain plot in figure 14. It should be noted that the values of the exponent m in table 4 are approximately double the values of m' in table 5; a consequence of the dependency of G and J on $\Delta\varepsilon^2$.

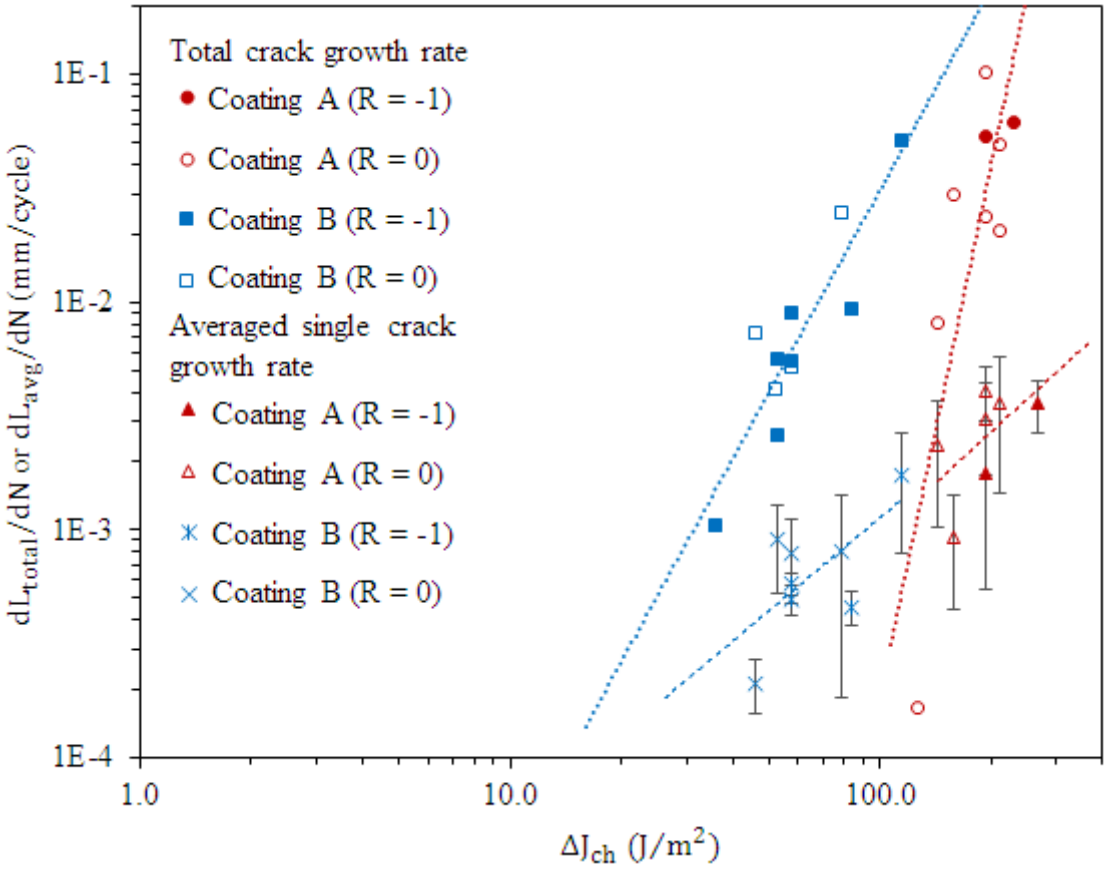

Figure 15. Total crack growth rate (dL_{total}/dN) and averaged non-interacting crack growth rates (dL_{avg}/dN) as a function of J-integral range (ΔJ_{ch}) for coatings A and B.

Coating type	dL_{total}/dN		dL_{avg}/dN	
	C (mm/cycle)	m	C (mm/cycle)	m
A	5.30×10^{-20}	7.77	1.02×10^{-6}	1.49
B	3.97×10^{-8}	3.03	2.14×10^{-6}	1.36

Table 5. Empirical constants of the lines in Figure 15 fitted using equation (12).

ΔJ has been shown to control rates of fatigue crack growth in both polymeric [28] and metallic [29] materials under non-linear deformation conditions, and by implication the same appears true of channelling crack growth.

In the region of life beyond the first 2 mm crack, cracking behaviour becomes more complex with crack interactions and continued increase in numbers of cracks. The corrosion protection offered by the coating to the substrate will steadily degrade with increasing length and number of through thickness cracks. Figure 10, 11 and 13 show that in both coating types, cycles to the onset of cracking and the rate at which new cracks are initiated are all dependent on the applied strain range.

A significant difference between the coatings was found in crack density and length. Coating A had a higher density of smaller cracks and coating B the converse with smaller numbers of longer cracks (Figure 11). A similar observation on cracking in static fracture was made by Wu *et al.* [15] in these coatings.

Coating A			Coating B		
Static failure strain (%)	Fatigue strain amplitude (%)	Normalised fatigue strain amplitude	Static failure strain %	Fatigue strain amplitude (%)	Normalised fatigue strain amplitude
1.04	0.43	0.41	0.64	0.23	0.36
	0.45	0.43		0.24	0.38
	0.5	0.48		0.25	0.39
	0.53	0.51		0.3	0.47

Table 6. Fatigue strain amplitudes of samples shown in Figure 11 normalised by coating static failure strains.

The different crack morphologies could be the result of coating B being tested at smaller strain amplitudes than coating A. However, Table 6 shows that although strain amplitudes are smaller for coating B than coating A, when strain amplitudes are normalised with respect to static failure strain of the two coatings, there is significant overlap in the normalised test strains. A few coating A samples were tested at smaller normalised strains than the largest normalised strain used for coating B. Despite this Figure 11 shows very different crack morphologies in all tested samples irrespective of the selected normalised strain amplitude. Unless the populations of starting defects in the two coatings are very different, it is difficult to account for the contrasting crack morphologies in terms of different test strain ranges.

An alternative explanation can be based on differences in the resistance of coatings to channelling crack development. Under conditions of static loading [15], the surface crack morphologies of coatings A and B samples are highly similar to those seen in the samples in the current work under fatigue conditions. At the onset of crack penetration through the thickness, it was estimated calculated that the strain energy release rate G_{ch} for crack channelling in coating A was less than the fracture toughness G_c, while for coating B, the G_{ch} values for channelling were always bigger than coating B toughness [15]. Therefore, in coating A extra cracks can initiate at the larger strain values required for crack channelling. In coating B cracks can channel as soon as they are initiated leading to a smaller number of larger cracks. This highlights a superior resistance of coating A samples to crack channelling than that of coating B samples, and this could also be the reason for the morphological differences between the coatings under fatigue conditions.

5. CONCLUSIONS

(1) Strain controlled fatigue tests have been performed on two types of filled epoxy anti-corrosion coatings nominally 300 µm thick on steel substrates. Cracking in both coatings proceeded via the

initiation and growth of coating cracks across the sample with crack numbers and crack length increasing as cycling progressed.

(2) Coating A with greater fracture toughness had smaller fatigue crack growth rates and a greater density of cracks, than the lower fracture toughness coating B which developed fewer longer cracks.

(3) Fatigue crack growth occupied the great majority of test life. At the beginning of the test cracking proceeded without crack to crack interactions and crack growth rate in individual cracks for a given strain range was a constant, independent of crack length. At longer lives and crack lengths greater than 2-4 mm, crack to crack interactions took place, reducing individual crack growth rates, while new cracks were continually initiated.

(4) Coating life could be defined as the cycles at which the first crack achieved 2 mm surface length. At this length cracking will be through the coating thickness and corrosion protection is first degraded. As cycling continues cracks become longer and more numerous and there will be a steady increase in the number and length of sites where the corrosive environment can access the substrate.

(5) Beyond the crack to crack interaction point the crack development process is accurately described by the total crack length, the sum of the lengths of all the cracks on the sample gauge length.

(6) Coating crack growth rates are strongly dependant on the applied strain range $\Delta\varepsilon^{m'}$, with m' values between 6 for coating B and 14 for coating A. A correlation of coating crack growth rates with ΔJ_{ch}, the J integral range for channelling cracks is demonstrated.

ACKNOWLEDGEMENTS

The authors would like to thank International Paint for financial and intellectual support. The thanks shall be extended to Dr Trevor Wills and Dr Paul Dooling at International Paint for their constructive advice; and to Mr Barry Walker at Cranfield University for his help in mechanical testing.

REFERENCES

[1] Sørensen PA, Kiil S, Dam-Johansen K, Weinell CE. Anticorrosive coatings: A review. Journal of Coatings Technology Research 2009;6:135–76.

[2] Wang G, Spencer JS, Saidarasamoot S, Thuanboon S, Olson DL, Mishra B. Tanker Corrosion. In: Kutz M, editor. Handbook of Environmental Degradation of Materials, Norwich, NY: William Andrew Publishing; 2005, p. 523–45. doi:10.1016/B978-081551500-5.50027-6.

[3] IMO. Performance standard for pretective coatings for dedicated seawater ballast tanks in all types of ships and double-side skin spaces of bulk carriers. Resolution MSC215(82) 2006.

[4] Lee D, Kim B. Investigation of coating failure on the surface of a water ballast tank of an oil tanker. Journal of Adhesion Science and Technology 2005;19:879–908. doi:10.1163/1568561054929946.

[5] Eve S, Huber N, Last a., Kraft O. Fatigue behavior of thin Au and Al films on polycarbonate and polymethylmethacrylate for micro-optical components. Thin Solid Films 2009;517:2702–7. doi:10.1016/j.tsf.2008.12.018.

[6] Sim GD, Lee YS, Lee SB, Vlassak JJ. Effects of stretching and cycling on the fatigue behavior of polymer-supported Ag thin films. Materials Science and Engineering A 2013;575:86–93. doi:10.1016/j.msea.2013.03.043.

[7] Kim B-J, Shin H-A-S, Jung S-Y, Cho Y, Kraft O, Choi I-S, et al. Crack nucleation during mechanical fatigue in thin metal films on flexible substrates. Acta Materialia 2013;61:3473–81. doi:10.1016/j.actamat.2013.02.041.

[8] Zhu D, Miller R a. Investigation of thermal fatigue behavior of thermal barrier coating systems. Surface and Coatings Technology 1997;94–95:94–101. doi:10.1016/S0257-8972(97)00484-2.

[9] Zhu DM, Choi SR, Miller RA. Development and fatigue testing of ceramic thermal barrier coatings. Surface and Coatings Technology 2004;188:146–52. doi:10.1016/j.surfcoat.2004.08.017.

[10] Zhang B, Kim B, Lee D. Stress analysis and evaluation of cracks developed on the coatings for welded joints of water ballast tanks. Corrosion 2005, Houston: NACE International; 2005, p. 1–10.

[11] Ringsberg JW, Ulfvarson AYJ. On mechanical interaction between steel and coating in stressed and strained exposed locations. Marine Structures 1998;11:231–50. doi:10.1016/S0951-8339(98)00015-X.

[12] Beuth JL. Cracking of thin bonded films in residual tension. International Journal of Solids and Structures 1992;29:1657–75. doi:10.1016/0020-7683(92)90015-L.

[13] Hutchinson JW, Suo Z. Mixed Mode Cracking in Layered Materials. Advances in Applied Mechanics 1991;29:63–191. doi:http://dx.doi.org/10.1016/S0065-2156(08)70164-9.

[14] Chai H. Channel cracking in inelastic film/substrate systems. International Journal of Solids and Structures 2011;48:1092–100. doi:10.1016/j.ijsolstr.2010.12.014.

[15] Wu T, Irving PE, Ayre D, Dell'Anno G, Jackson P, Zhao F. Fracture of epoxy-based marine coatings as free films and substrated coatings under static tension. Engineering Fracture Mechanics 2016;159:1–15. doi:10.1016/j.engfracmech.2016.02.048.

[16] Hoffman RW. Stress distributions and thin film mechanical properties. Surface and Interface Analysis 1981;3:62–6. doi:10.1002/sia.740030113.

[17] Wu T. Investigation of the fracture behaviour of epoxy-based water ballast tank coatings under static and fatigue loadings (PhD thesis). Cranfield University, 2015.

[18] British Standards Institute. ISO 8501-1:2007 Preparation of steel substrates before application of paints and related products - Visual assessment of surface cleanliness - Part 1: Rust grades and preparation grades of uncoated steel substrates and of steel substrates after overa. ISO Standard 2007:74.

[19] Yan G, White JR. Residual stress development in a bi-layer coating. Polymer Engineering & Science 1999;39:1856–65. doi:10.1002/pen.11579.

[20] Lei H, Francis LF, Gerberich WW, Scriven LE. Stress development in drying coatings after solidification. AIChE Journal 2002;48:437–51. doi:10.1002/aic.690480304.

[21] Perera DY. Physical ageing of organic coatings. Progress in Organic Coatings 2003;47:61–76. doi:10.1016/S0300-9440(03)00037-7.

[22] Suresh S. Fatigue of Materials. Cambridge: Cambridge University Press; 1998. doi:10.1017/CBO9780511806575.

[23] Xia ZC, Hutchinson JW. Crack patterns in thin films. Journal of the Mechanics and Physics of Solids 2000;48:1107–31. doi:10.1016/S0022-5096(99)00081-2.

[24] Paris P, Erdogan F. A Critical Analysis of Crack Propagation Laws. Journal of Basic Engineering 1963;85:528. doi:10.1115/1.3656900.

[25] Sutton S a. Fatigue crack propagation in an epoxy polymer. Engineering Fracture Mechanics 1974;6:587–95. doi:10.1016/0013-7944(74)90015-0.

[26] Bak BL V., Sarrado C, Turon A, Costa J. Delamination Under Fatigue Loads in Composite Laminates: A Review on the Observed Phenomenology and Computational Methods. Applied Mechanics Reviews 2014;66:60803. doi:10.1115/1.4027647.

[27] Dundurs J. Edge-Bonded Dissimilar Orthogonal Elastic Wedges Under Normal and Shear Loading. Journal of Applied Mechanics 1969;36:650. doi:10.1115/1.3564739.

[28] Kuronuma Y, Shindo Y, Takeda T, Narita F. Crack growth characteristics of carbon nanotube-based polymer composites subjected to cyclic loading. Engineering Fracture Mechanics 2011;78:3102–10. doi:10.1016/j.engfracmech.2011.09.006.

[29] Dowling NE, Begley J a. Fatigue crack growth during gross plasticity and the J-integral. ASTM Special Technical Publication 1976:82–103.

[30] Lamba HS. The J-integral applied to cyclic loading. Engineering Fracture Mechanics 1975;7:693–703. doi:10.1016/0013-7944(75)90025-9.

[31] Dowling NE, Impellizzeri LF. Crack Growth During Low-Cycle Fatigue of Smooth Axial Specimens. ASTM Special Technical Publication 1977:97–121.

[32] ABAQUS. Documentation. vol. 6.11. Providence, RI, USA: Dassault Systemes Simulia Corp; 2011.

Fatigue cracking behaviour of epoxy-based marine coatings on steel substrate under cyclic tension

Wu, Tongyu

2017-02-13

Wu T, Irving P, Ayre D, Jackson P, Zhao F, Fatigue cracking behaviour of epoxy-based marine coatings on steel substrate under cyclic tension, International Journal of Fatigue, Volume 99, Part 1, June 2017, Pages 13–24.

http://dx.doi.org/10.1016/j.ijfatigue.2017.02.010